IEEE Photonics Journal
An IEEE Photonics Society Publication

Open Access

Support Vector Machine based Differential Pulse-width Pair Brillouin Optical Time Domain Analyzer

Volume 10, Number 4, August 2018

Huan Wu
Liang Wang
Zhiyong Zhao
Chester Shu
Chao Lu

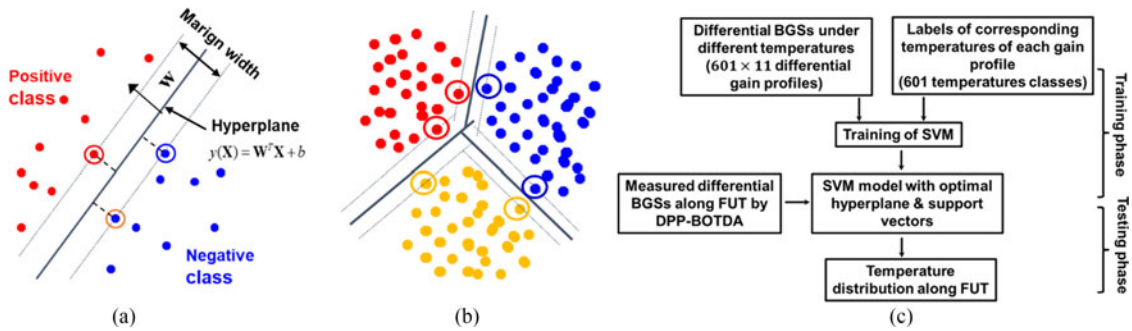

DOI: 10.1109/JPHOT.2018.2858235
1943-0655 © 2018 IEEE

IEEE photonics SOCIETY

IEEE

Support Vector Machine based Differential Pulse-width Pair Brillouin Optical Time Domain Analyzer

Huan Wu,[1] Liang Wang,[1] Zhiyong Zhao,[2] Chester Shu,[1] and Chao Lu [2]

[1]Department of Electronic Engineering, The Chinese University of Hong Kong, Shatin, Hong Kong
[2]Department of Electronic and Information Engineering, The Hong Kong Polytechnic University, Kowloon, Hong Kong

DOI:10.1109/JPHOT.2018.2858235

Manuscript received March 6, 2018; revised June 24, 2018; accepted July 18, 2018. Date of publication July 23, 2018; date of current version July 31, 2018. This work was supported by the Research Grants Council of Hong Kong project: CUHK GRF 14206614, 14238816, 14209517, PolyU 5208/13E, 15265816, 15216817; and by the National Natural Science Foundation of China under Grants 61377093, 61435006, and U1701661. Corresponding author: Liang Wang (e-mail: lwang@ee.cuhk.edu.hk).

Abstract: Support vector machine (SVM) based differential pulse-width pair Brillouin optical time domain analyzer (DPP-BOTDA) has been proposed and experimentally demonstrated. With only one SVM model, temperature distribution along 5 km fiber under test has been successfully extracted from differential Brillouin gain spectrum (BGS) measured under different spatial resolution in DPP-BOTDA. The temperature accuracy by SVM is better than that by Lorentzian curve fitting (LCF), especially when the pump pulse width difference and the number of trace averaging used in the measurement are small, indicating larger tolerance of SVM to high spatial resolution and low signal-to-noise ratio. SVM is also more robust to a wide range of frequency scanning steps and has less accuracy degradation under large frequency scanning step. To extract temperature from 50 000 differential BGSs, 133.17 and 1.12 s are consumed by SVM-0.1 and SVM-1 °C, respectively, both of which are much shorter than that by LCF. The data processing time of SVM is further shortened with the help of principle component analysis for data dimension reduction. SVM for measurand extraction would be especially helpful in the scenario of DPP-BOTDA where high data sampling rate is required to resolve plenty of submeter scale sensing points.

Index Terms: Brillouin optical time domain analyzer, differential pulse-width pair, support vector machine, temperature extraction, data processing time.

1. Introduction

Over the past three decades, intensive research interest has been given to Brillouin optical time domain analyzer (BOTDA), which can achieve long-range distributed temperature and strain monitoring in a cost-effective way [1], [2]. Plenty of techniques have been developed to enhance the accuracy and spatial resolution, to enlarge the measurement range, and to improve the measurement speed [3]–[5]. In conventional BOTDA, the duration of pump pulse determines the measurement spatial resolution, which is limited by the acoustic phonon lifetime, i.e., ∼10 ns, corresponding to

1-meter spatial resolution. In many applications such as structural health monitoring, sub-meter spatial resolution is desirable for the detection of small changes. Several schemes have been proposed to realize sub-meter spatial resolution, including the use of dark pulse [6], the pre-pumping technique [7], Brillouin dynamic grating [8] and differential pulse-width pair BOTDA (DPP-BOTDA) [9], [10], etc. Among these techniques, DPP-BOTDA has been demonstrated to be an excellent method for long-distance distributed sensing with sub-meter spatial resolution [11]–[18]. In DPP-BOTDA, two cycles of measurement are carried out in sequence over the fiber, with two pump pulses of slightly different duration used for each cycle. The differential Brillouin gain spectrum (BGS) is obtained by subtraction between two conventional BOTDA traces excited by the two pump pulses, and the local Brillouin frequency shift (BFS) is retrieved at a spatial resolution determined by the pulse duration difference. Like in conventional BOTDA, curve fitting methods are usually used to estimate the BFS from the differential BGS, and the BFS is taken as the frequency of the peak gain on the fitted curves [11], [12], [17], [18]. However, curve fitting needs algorithm iteration to fit the differential BGS, which takes long time to extract BFS, especially for the case of denser sensing points in DPP-BOTDA due to sub-meter spatial resolution over tens of kilometers distance. Moreover, the data acquisition in DPP-BOTDA is usually implemented at high sampling rate in order to resolve sub-meter scale changes, which also leads to longer data processing time by conventional curve fitting. Poor initialization of model parameters in curve fitting will also significantly deteriorates the accuracy of BFS estimation [19]. Besides curve fitting methods, Artificial Neural Network (ANN) has also been proposed to extract temperature information from the BGS in a BOTDA system [20], [21]. But ANN usually requires lots of empirical trails and hence time in order to find a suitable architecture in the training phase.

Recently we have reported the use of Support Vector Machine (SVM) in conventional BOTDA to directly extract temperature with faster speed and better accuracy than conventional curve fitting methods [22], [23]. In [22], besides better accuracy, SVM exhibits a data processing speed faster than the commonly used Lorentzian curve fitting (LCF) by two orders of magnitude. To broaden the application range of SVM for measurand extraction, it is essential to examine its feasibility and performance in BOTDA configurations which have different gain profiles from that of conventional BOTDA, such as DPP-BOTDA. Furthermore, in DPP-BOTDA, the signal-to-noise ratio (SNR) is usually lower than that in conventional BOTDA due to the differential operation, thus the SVM based DPP-BOTDA to achieve better accuracy of measurand extraction would be more attractive than the curve fitting based counterpart. In order to make SVM feasible for the measurand extraction in DPP-BOTDA, the SVM model should be trained using appropriately designed training data. In this paper, we investigate the temperature extraction by SVM in DPP-BOTDA to improve the sensing accuracy and accelerate the data processing speed. We design appropriate training data suitable for SVM training in the scenario of temperature extraction from differential BGSs, and experimentally analyze the performance of SVM in DPP-BOTDA under different experiment conditions. Our results show that SVM has better temperature accuracy than LCF especially at low SNR, which is more desirable for the measurement in DPP-BOTDA. We also analyze the data processing time using SVM for temperature extraction under different pump pulse pairs and different temperature steps, which is shown to be much shorter than that using LCF. Finally for the first time, we apply Principle Component Analysis (PCA) to reduce the data dimension of differential BGSs in both training and testing phases of SVM, and hence achieve further reduction of data processing time without degradation of measurement accuracy.

2. Principle of SVM and Its Training for Temperature Extraction in DPP-BOTDA

SVM serves as a discriminative classifier to distinguish different classes, and it is remarkably robust to sparse and noisy data, which makes it have many applications, e.g., text categorization and protein function prediction [24]. The working principle of classification by SVM is described in Fig. 1. The vector of input data sample is expressed as $X_i = (x_1, x_2, \ldots, x_M)$, where M is the

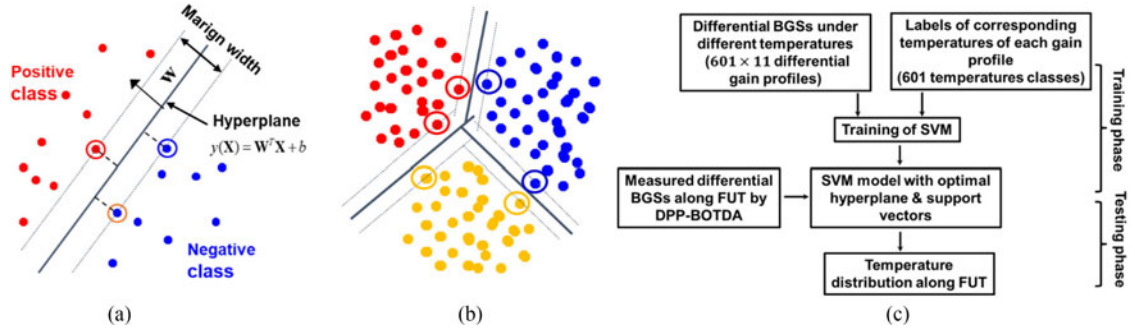

Fig. 1. (a) Two-class classification by SVM; (b) multi-class classification by SVM; (c) SVM for temperature extraction in DPP-BOTDA.

number of vector dimension and $i = 1, 2, \ldots, N$ is the sequence of the data sample. In Fig. 1(a), there are two classes for all the data samples, i.e., positive class (red dots) and negative class (blue dots). The labels for positive and negative classes are $l = 1$ and $l = -1$, respectively. The decision function for the data sample X_i is constructed based on the sign of $f(X) = W^T X + b$ as follows:

$$sign\,(f\,(X_i)) > 0 \rightarrow l_i = 1 \rightarrow X_i\ belongs\ to\ the\ positive\ class$$

$$sign\,(f\,(X_i)) < 0 \rightarrow l_i = -1 \rightarrow X_i\ belongs\ to\ the\ negative\ class$$

W is a norm vector and b is the scalar intercept. In the case of linearly separable data, it is possible to find a hyperplane satisfying the following condition, which can be used to classify each data sample into either positive class or negative class:

$$f\,(X) - W^T X - b = 0$$

The values of W and b give the position of the hyperplane. To separate and classify the input data samples, SVM tries to find an optimal hyperplane, which has the maximum margin between itself and the nearest data samples, i.e., support vectors, shown as the circled red and blue dots in Fig. 1(a). In the training phase of SVM, the norm vector W and intercept b are determined through the learning from training data samples, with a goal to maximize the margin width and hence find the optimal hyperplane and support vectors. After training, all the necessary information needed to construct the SVM classifier is contained in the optimal hyperplane and support vectors. In the testing phase, the SVM model is used to classify the testing data samples according to the optimal hyperplane and support vectors.

In Fig. 1(a), only two classes exist and binary classification by SVM is enough. In practical situations, however, many problems involve classification of multiple classes, e.g., 3 classes in Fig. 1(b). For multi-classification by SVM, here we adopt one-against-one method [22], [25]. This method constructs $k(k-1)/2$ binary classifiers for a problem with k classes, and each binary classifier is trained to distinguish the samples from one class with the other class in each pair of classes. For example, in Fig. 1(b), three classes are represented by red, blue and yellow dots, respectively. To classify them, three binary classifiers are constructed with hyperplanes and corresponding support vectors formed between the red and blue classes, red and yellow classes, and blue and yellow classes, respectively. After the classification by all the three binary classifiers, the testing data sample is classified to the class which wins the maximum voting process [22].

The training and testing phases of a linear multi-class SVM classifier for temperature extraction in DPP-BOTDA is shown in Fig. 1(c). Within the temperature range from 10 °C to 70 °C, 601 temperature classes are formed at a temperature step of 0.1 °C. In the training phase, ideal differential BGSs together with the labels of corresponding temperature classes serve as the training data samples to determine the optimal hyperplane and support vectors of the SVM model for

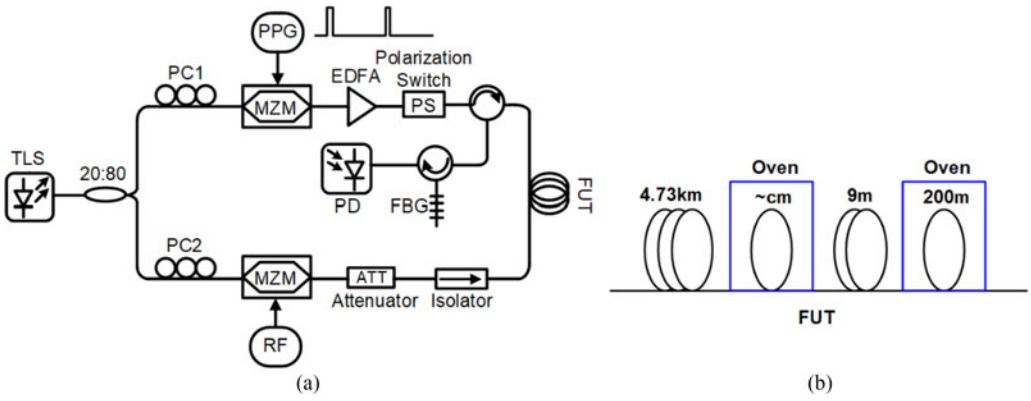

Fig. 2. (a) Experiment setup of DPP-BOTDA; (b) 5 km long FUT with two heated sections. TLS: tunable laser source, PC: polarization controller, PPG: pulse pattern generator, RF: radio frequency, PS: polarization switch, MZM: Mach-Zehnder modulator, FUT: fiber under test, FBG: fiber-Bragg grating, PD: photodetector.

temperature extraction. We design the ideal differential BGSs by using Lorentzian curve as the gain profile of differential BGSs for the training of SVM:

$$g(v) = g_B \frac{1}{1 + [(v - v_B)/(\Delta v_B/2)]^2}$$

where g_B, υ_B, and $\Delta\upsilon_B$ are the gain peak, BFS and bandwidth of the differential BGS. The BFSs of ideal differential BGSs are determined using the calibrated temperature coefficient of 0.9749 MHz/ °C for our fiber under test (FUT). As the differential BGS in DPP-BOTDA is obtained by subtraction between two conventional BGSs excited by two pump pulses of slight duration difference, its bandwidth cannot be directly estimated using the pulse duration, unlike the case in [22] where the bandwidth of the ideal conventional BGS is assumed to be inversely proportional to the pulse duration, e.g., 100 MHz for ~10 ns pulse duration. Here we estimate the bandwidth of ideal differential BGSs based on experiment. We collect differential BGSs by DPP-BOTDA using pump pulse pairs with pulse duration difference from 2 ns to 10 ns, and find that the bandwidth range of ideal differential BGSs can be set to within 20 MHz ~ 40 MHz, which is enough to accommodate the bandwidth variation of differential BGSs along FUT during measurement. So for each temperature class, we obtain ideal differential BGSs with the same BFS but different bandwidth varying from 20 MHz to 40 MHz at a step of 2 MHz. Finally, we have 601 × 11 ideal differential gain profiles to train the SVM. The frequency range of υ is from 10.75 GHz to 10.95 GHz, the same as the frequency scanning range during the acquisition of differential BGSs. In the testing phase, the measured differential BGSs along FUT are processed by the SVM model with the optimal hyperplane and support vectors. And the temperature distribution along FUT is obtained after each differential BGS is classified into one of the temperature classes, as shown in Fig. 1(c).

3. Experiment and Results

3.1 Temperature Extraction by SVM in DPP-BOTDA under Different Experiment Conditions

The DPP-BOTDA experiment setup is shown in Fig. 2(a). The output of a tunable laser at 1550 nm is split into two branches using a 20/80 coupler. The optical pump pulse pair including two pump pulses of different pulse duration is generated in the upper branch through optical modulation by a Mach-Zehnder modulator (MZM) of 40 dB extinction ratio. The electrical pulse pair injected into the modulator is provided by a programmable pulse pattern generator. After passing through an erbium-doped fiber amplifier (EDFA) and a polarization switch (PS), the pump pulse pair is delivered to the fiber under test (FUT). In the lower branch, a double-sideband probe signal is generated by

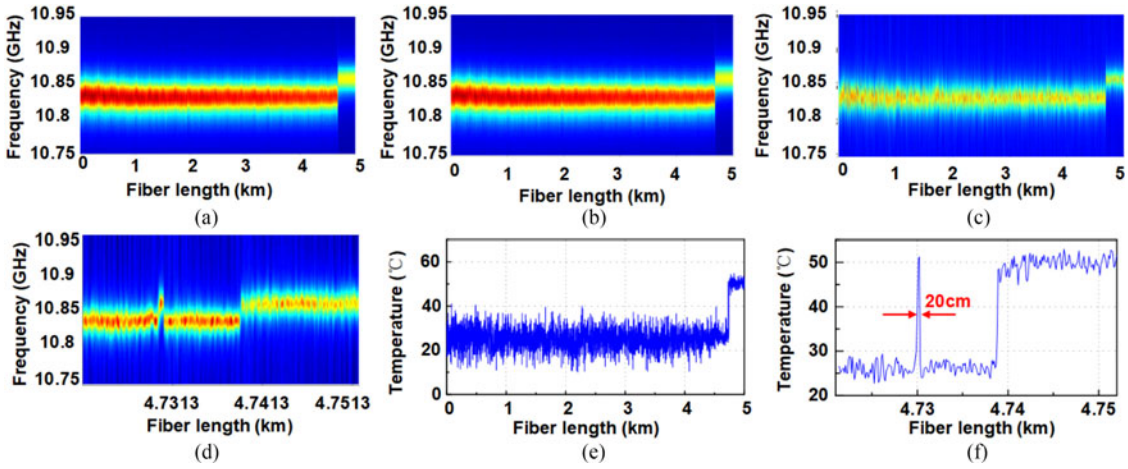

Fig. 3. (a) and (b) BGS distribution along FUT measured by using single 50 ns pump pulse and 48 ns pump pulse, respectively; (c) differential BGS distribution along FUT obtained by subtraction of BGSs in (a) and (b); (d) zoom-in view of differential BGS distribution near the fiber end; (e) temperature distribution extracted by SVM from the differential BGS and (f) zoom-in view near the fiber end.

carrier suppression modulation using another high-extinction ratio MZM, which is driven by a RF signal. The probe is amplified in FUT by the pump pulse pair and two adjacent probe traces excited by each pump pulse of one pair are detected and collected on an oscilloscope after the unwanted probe sideband is removed by using a fiber Bragg grating (FBG). The differential trace is obtained by subtraction between the two adjacent traces. The frequency of the RF signal is scanned from 10.75 GHz to 10.95 GHz for differential BGS reconstruction. In the experiment, the FUT is a 5 km long single mode fiber, as shown in Fig. 2(b). A short section (∼cm long) at the location of 4.73 km and a long section (200 m long) at the FUT end are put inside ovens and heated to 50 °C. The short heated section has a length equal to the theoretical spatial resolution of DPP-BOTDA, which is used to examine the detection of sub-meter hot-spot. While the long heated section has a fixed length of 200 m, and is used to evaluate the measurement accuracy (e.g., temperature uncertainty). The sampling rate for data acquisition is 1GSample/s, corresponding to 2000 sensing points along the last 200 m section, which offers sufficient data points to analyze the statistical performance of SVM.

To analyze the performance of SVM to extract temperature in DPP-BOTDA of different spatial resolution, we measure the differential BGS by using different pump pulse pairs, i.e., 50/48 ns, 50/47 ns, 50/46 ns, 50/45 ns, 50/44 ns, 50/43 ns, 50/42 ns, 50/41 ns and 50/40 ns, respectively. The above pump pulse pairs correspond to spatial resolution of 20 cm ∼ 100 cm at a step of 10 cm. Accordingly, we make the length of the short heated section vary from 20 cm to 100 cm with a step of 10 cm. Taking the 50/48 ns pump pulse pair as an example, in Figs. 3(a)–(b) we show the BGS distribution along FUT measured with single 50 ns pump pulse and 48 ns pump pulse, respectively. 1024 averaging times and 1 MHz frequency scanning step are adopted for the measurement. For single-pump BOTDA, the spatial resolution of 5 m and 4.8 m are much longer than the length of the 20 cm short heated section, so only the last 200 m heated section is detected. On the other hand, Fig. 3(c) depicts the differential BGS distribution obtained from the subtraction between BGSs in Figs. 3(a) and (b), and its zoom-in view near the fiber end is given in Fig. 3(d). We can see that both the 20 cm and 200 m heated sections have been detected. The measured differential BGSs are processed by the SVM after training and the temperature along FUT has been successfully extracted without the need of conversion between BFS and temperature, as shown in Fig. 3(e). Fig. 3(f) plots the zoom-in view of Fig. 3(e) near the fiber end, where the 20 cm heated section at the location of 4.73 km and the last 200 m heated section are clearly observed. The temperature uncertainty, defined as the standard deviation of the extracted temperature, is calculated to be 2.22 °C at the FUT end. The results using other pump pulse pairs are given in Figs. 4(a)–(h), where

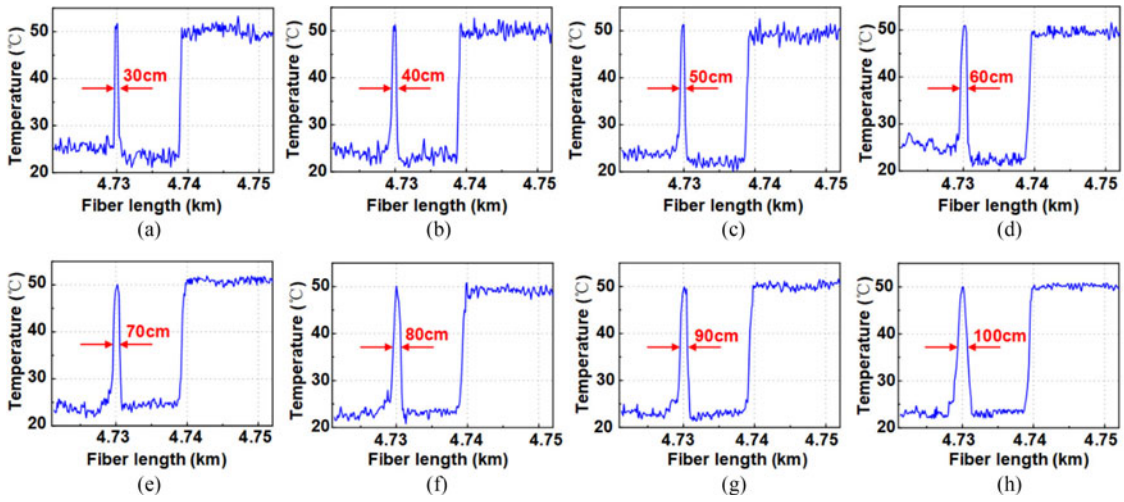

Fig. 4. Temperature distribution near the fiber end extracted by SVM from differential BGSs measured using pump pulse pair of (a) 50/47 ns, (b) 50/46 ns, (c) 50/45 ns, (d) 50/44 ns, (e) 50/43 ns, (f) 40/42 ns, (g) 50/41 ns and (h) 50/40 ns, respectively. The corresponding length of the short heated section at the location of 4.73 km is varied from 20 cm to 100 cm at a step of 10 cm, respectively.

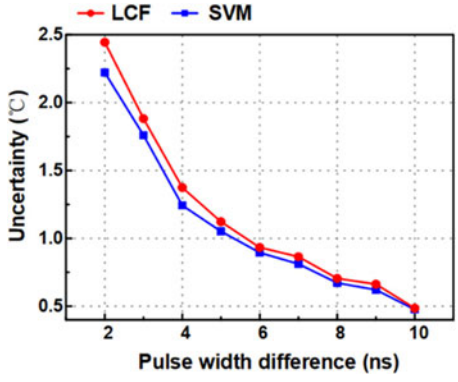

Fig. 5. Temperature uncertainty versus pulse width difference. The number of trace averaging is 1024.

the temperature distribution near the fiber end extracted by the same SVM model is given. Note that in the experiment for each pump pulse pair, the length of the short heated section at the location of 4.73 km is made equal to the corresponding theoretical spatial resolution. We can see that the temperatures along FUT including both the short and long heated sections are exactly extracted by SVM under different spatial resolution of DPP-BOTDA. Fig. 4 indicates that one SVM model is enough and feasible to extract temperature from differential BGSs measured with different spatial resolution in DPP-BOTDA. In Fig. 4, when the pump pulse width difference increases from 3 ns to 10 ns, the temperature uncertainty by SVM at FUT end is improved from 1.76 °C to 0.47 °C. And Fig. 5 shows the uncertainty versus pulse width difference. As comparison, we also plot the results by using LCF for temperature extraction. Both the uncertainty using SVM and LCF decreases as the pulse width difference increases, which is due to the better signal-to-noise ratio (SNR) achieved when larger pulse width difference is used for measurement. But for each pulse width difference, the uncertainty by SVM is found to be lower than that by LCF, especially when the pulse width difference becomes small. It indicates that SVM has larger tolerance to the pulse width difference and thus still works better than LCF in DPP-BOTDA of higher spatial resolution. Note that our experiment setup is similar to that in [9], except the use of a single laser for stability, which leads to slightly better temperature uncertainties compared with those in [9].

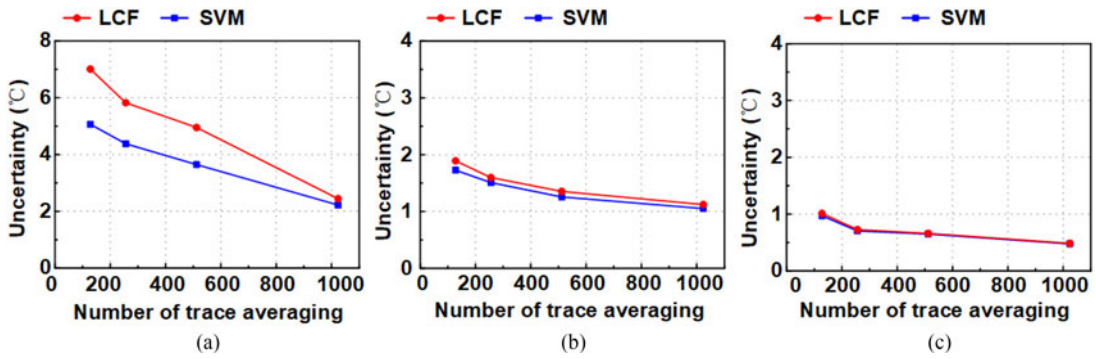

Fig. 6. Temperature uncertainty by SVM versus number of trace averaging for pump pulse pairs of (a) 50/48 ns, (b) 50/45 ns and (c) 50/40 ns, respectively.

We also investigate the tolerance of SVM to the number of trace averaging in DPP-BOTDA. The differential BGSs are collected under different number of trace averaging, i.e., 128, 256, 512, and 1024. The frequency scanning step is fixed at 1 MHz. Larger number of trace averaging gives rise to higher SNR of the trace. Figs. 6(a)–(c) show the temperature uncertainty by both SVM and LCF as a function of number of trace averaging for three pump pulse pairs, i.e., 50/48 ns, 50/45 ns and 50/40 ns, respectively. The temperature uncertainty is calculated using the extracted temperature at the last 200 m heated section. The uncertainty by both SVM and LCF decreases as the averaging times are increased. For the pump pulse pair of 50/48 ns, corresponding to spatial resolution of 20 cm, the uncertainty by SVM is obviously smaller than that by LCF, especially when the number of trace averaging is low, as shown in Fig. 6(a). For example, when the number of trace averaging is 128, the uncertainty by SVM is 5.06 °C, while that by LCF is 7.01 °C. It implies that SVM is more robust to the number of trace averaging and SNR, and thus it still has better accuracy than LCF at low averaging times and low SNR in DPP-BOTDA. On the other hand, in Fig. 6(b) and Fig. 6(c), when the pulse width difference becomes larger such as 5 ns and 10 ns, the uncertainty by SVM becomes comparable to that by LCF, regardless of the number of trace averaging. This is because the SNR becomes higher when the pulse width difference increases, i.e., lower spatial resolution. For the pump pulse pair of 50/40 ns, which corresponds to spatial resolution of 1 m, the SNR is much better than the case of 50/48 ns pulse pair, even under small number of trace averaging. Therefore, for large pulse width difference leading to high SNR, SVM has similar performance to LCF; while for small pulse width difference giving rise to low SNR, SVM exhibits better accuracy than LCF. It implies that SVM for temperature extraction is especially helpful to achieve better accuracy in DPP-BOTDA where low SNR exists at high spatial resolution.

Next we change the frequency scanning step to collect differential BGSs in DPP-BOTDA in order to evaluate the accuracy by SVM under different frequency scanning steps. Several frequency scanning steps (i.e., 1 MHz, 2 MHz, 5 MHz, 10 MHz, 15 MHz) are adopted for the measurement of differential BGSs. The number of trace averaging is fixed at 1024. Figs. 7(a)–(c) show the temperature uncertainty by SVM and LCF as a function of frequency scanning step for three pump pulse pairs (i.e., 50/48 ns, 50/45 ns and 50/40 ns), respectively. As the frequency step increases, fewer data points are collected on each differential BGS, resulting in degradation of uncertainty by both SVM and LCF. However, the uncertainty by SVM degrades more slowly than that by LCF as the frequency step increases, and hence SVM gives lower uncertainty, especially when the pulse width difference is smaller, e.g., 13.5 °C uncertainty by SVM compared with 22.3 °C by LCF for 50/48 ns pulse pair at 15 MHz frequency step, as shown Fig. 7(a). SVM is trained to obtain the knowledge of differential BGSs before it is used for temperature extraction, thus the reduction of data points on each differential BGS has less effect on SVM, unlike LCF which strongly relies on the number of data points for curve fitting. Fig. 7 indicates that SVM can better adapt a wide range of frequency steps in DPP-BOTDA than LCF does.

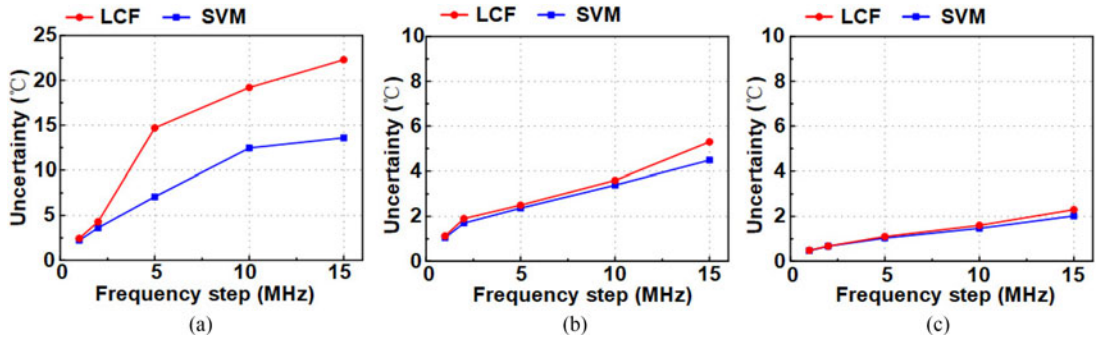

Fig. 7. Temperature uncertainty by SVM versus frequency scanning step for pump pulse pairs of (a) 50/48 ns, (b) 50/45 ns and (c) 50/40 ns, respectively.

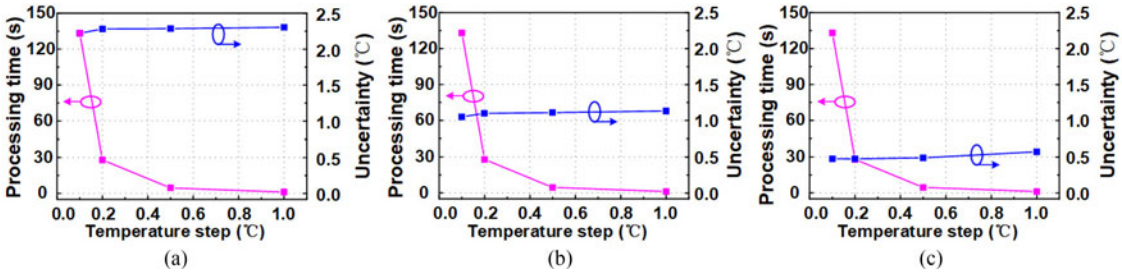

Fig. 8. Data processing time and temperature uncertainty by SVM versus temperature step for pump pulse pairs of (a) 50/48 ns, (b) 50/45 ns and (c) 50/40 ns, respectively.

3.2 Analysis of Data Processing Time of SVM

In this section, we analyze the data processing time of temperature extraction using SVM in DPP-BOTDA. In the previous section, 601 temperature classes are formed at a step of 0.1 °C for temperature extraction using SVM. Since the data processing time of SVM is related to the number of temperature classes, here we also use 0.2 °C, 0.5 °C and 1 °C steps to form 301, 121 and 61 temperature classes, respectively. Then four corresponding SVM models, i.e., SVM-0.1 °C, SVM-0.2 °C, SVM-0.5 °C, and SVM-1 °C are separately trained to extract the temperature from the same differential BGSs measured by DPP-BOTDA. The differential BGSs along 5 km FUT are collected using 1 MHz frequency scanning step (i.e., 200 scanned frequencies), 1024 averaging times and 1GSample/s sampling rate. Thus there are 50,000 sensing points along 5 km FUT and the total number of data points to process by SVM is $50,000 \times 200$. Fig. 8 plots the data processing time of temperature extraction by SVM as a function of temperature step, when three pump pulse pairs are used to collect the differential BGSs, respectively. The data processing time using SVM decreases quickly as the temperature step increases. For all the three pump pulse pairs, SVM-0.1 °C requires almost the same ~133.17s to extract temperature from 50,000 differential BGSs, while SVM-1 °C only consumes ~1.12s to process the same data. As mentioned above, SVM adopts one-against-one strategy for multi-class classification, where it constructs $k(k-1)/2$ binary classifiers for k classes. So there are 180300 binary classifiers for 601 classes formed at a temperature step of 0.1 °C, while this number of binary classifiers is reduced to only 1830 for 61 classes at a temperature step of 1 °C, resulting in significant reduction of the processing time for SVM-1 °C. The corresponding temperature uncertainty for temperature steps is also calculated in Fig. 8. The uncertainty only has little degradation as the temperature step increases from 0.1 °C to 1 °C, e.g., 2.22 °C for 0.1 °C temperature step and 2.30 °C for 1 °C temperature step in the case of 50/48ns pulse pair. Thus one can use 1 °C step to form temperature classes and subsequently extract temperature by SVM-1 °C at fast speed but without much sacrifice of the accuracy. It is

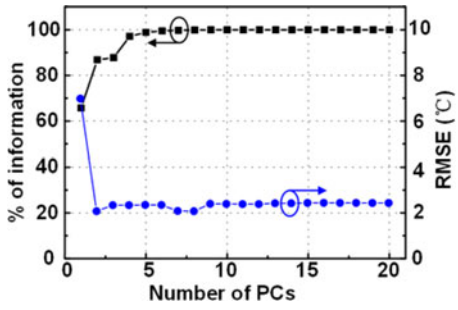

Fig. 9. Percentage of information contained in the chosen PCs and RMSE versus number of PCs. The data for pump pulse pairs of 50/48 ns with 1024 times averaging and 1 MHz frequency scanning step is used for analysis.

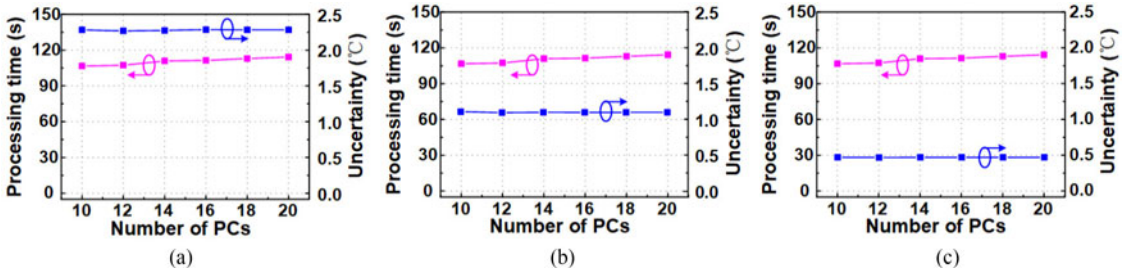

Fig. 10. Reduced data processing time and temperature uncertainty of SVM versus number of principle components for pump pulse pairs of (a) 50/48 ns, (b) 50/45 ns and (c) 50/40 ns, respectively.

worth mentioning that the data processing time by LCF is found to be dependent on the pulse width difference used for differential BGSs measurement, e.g., 693.55 s for 50/48 ns pair, 652.51 s for 50/45 ns pair, and 606.83s for 50/40 ns pair to process the same 50,000 differential BGSs. This is because curve fitting relies more on the quality of the measured differential BGS and more time is needed for algorithm iteration to fit the noisy differential BGS, like that in the case of 50/48 ns pair. Even for the case of 50/40 ns pair, SVM-0.1 °C and SVM-1 °C are still beyond 4 times and 500 times faster than LCF, respectively.

The data processing by SVM can be further accelerated by reducing the data dimension of differential BGSs based on Principle Component Analysis (PCA). PCA can identify the most meaningful basis of original data to re-express the data set [26]. By calculating the eigenvectors of the covariance matrix of the original input data, PCA linearly transforms a high-dimensional input vector into a low-dimensional one whose components are uncorrelated. We apply PCA to differential BGSs in both training and testing phases of SVM to achieve the data dimension reduction [27], [28]. Since SVM-0.1 °C consumes the most time among other SVMs, we use it as an example to demonstrate further reduction of data processing time of SVM based on PCA. To study the number of PCs needed for the data dimension reduction, we first analyze the percentage of information contained in the selected PCs, as shown in Fig. 9. The percentage of information contained in the selected PCs increases as the number of PCs increases. When the number of PCs increases to 5, it contains almost all the original data information. Fig. 9 also indicates that the temperature root mean square error (RMSE) decreases quickly as the number of PCs increases, and it becomes stable when the number of PCs is larger than 10. Note that in order to avoid significant degradation of temperature accuracy due to the reduced data dimension by PCA, we make the number of PCs have a value from 10 to 20. Fig. 10 shows the reduced data processing time to extract temperature by SVM-0.1 °C as a function of the number of principle components (PCs). PCA has been used to reduce the data dimension of differential BGSs for three pump pulse pairs, respectively. The differential BGSs are the same as those in Fig. 8 for the case of 0.1 °C temperature step. For all the pump pulse pairs, the data processing time to extract temperature from 50,000 differential BGSs

by SVM-0.1 °C is reduced to the range of 106.6 s ∼ 114.2 s, depending on the number of PCs (10 ∼ 20). Without PCA (i.e., 200 dimensions), this time is 133.17 s. As shown in Fig. 10, when the data dimension varies from 10 to 20, the temperature uncertainty maintains almost the same because the number of PCs used to represent the original differential BGSs is sufficient to avoid temperature degradation. With fewer PCs, the data processing speed is faster, but the accuracy will become worse.

4. Conclusion

We have successfully demonstrated the use of SVM for temperature extraction in DPP-BOTDA, and analyzed its performance under various experimental conditions. Differential BGSs are collected using different pump pulse pairs along 5 km FUT by DPP-BOTDA and then processed by SVM trained using the designed differential BGSs. At spatial resolution of 20 cm to 100 cm, the temperature distribution along FUT including both short and long heated sections has been exactly extracted by using only one SVM model without the need of conversion between BFS and temperature. Compared with LCF, SVM has larger tolerance to the pulse width difference and the number of trace averaging used in the measurement of differential BGSs. Hence it shows better accuracy of temperature extraction, especially when the spatial resolution is high and the number of trace averaging is small. Due to the knowledge obtained in the training phase, SVM well adapts a wide range of frequency scanning steps for the collection of differential BGSs, and has less degradation of measurement accuracy than LCF when large frequency scanning step is used in DPP-BOTDA. The data processing time of SVM is found to be strongly dependent on the temperature step used to form temperature classes, rather than on the pump pulse width difference, which is unlike that of LCF. To extract temperature from 50,000 differential BGSs, SVM-0.1 °C requires ∼133.17 s, while SVM-1 °C only consumes ∼1.12 s without much accuracy degradation. In comparison to the time by LCF (e.g., 606.83 s for 50/40 ns pair), the one by SVM is much shorter. Moreover, with the data dimension of differential BGSs reduced by PCA and temperature accuracy maintained, the data processing time of SVM-0.1 °C is further reduced to the range of 106.6 s ∼ 114.2 s. We believe SVM for temperature extraction would be exceptionally desirable in DPP-BOTDA sensors where a large number of sensing points are to be resolved at high resolution, high accuracy and fast speed [29].

References

[1] C. A. Galindez-Jamioy and J. M. Lopez-Higuera, "Brillouin distributed fiber sensors: An overview and applications," *J. Sens.*, vol. 2012, 2012, Art. no. 204121.
[2] A. Motil, A. Bergman, and M. Tur, "State of the art of Brillouin fiber-optic distributed sensing," *Opt. Laser Technol.*, vol. 78, pp. 81–103, 2016.
[3] D. Zhou *et al.*, "Slope-assisted BOTDA based on vector SBS and frequency-agile technique for wide-strain-range dynamic measurements," *Opt. Exp.*, vol. 25, no. 3, pp. 1889–1902, 2017.
[4] A. Denisov, M. Soto, and L. Thévenaz, "Going beyond 1000000 resolved points in a Brillouin distributed fiber sensor: theoretical analysis and experimental demonstration," *Light Sci. Appl.*, vol. 5, no. 5, 2016, Art. no. e16074.
[5] Y. Mizuno, N. Hayashi, H. Fukuda, K. Song, and K. Nakamura, "Ultrahigh-speed distributed Brillouin reflectometry," *Light: Sci. Appl.*, vol. 5, no. 12, 2016, Art. no. e16184.
[6] A. W. Brown, B. G. Colpitts, and K. Brown, "Dark-pulse Brillouin optical time-domain sensor with 20-mm spatial resolution," *J. Lightw. Technol.*, vol. 25, no. 1, pp. 381–386, Jan. 2007.
[7] K. Kishda, C. Li, and K. Nishiguchi, "Pulse pre-pump method for cm-order spatial resolution of BOTDA," in *Proc. SPIE*, 2005, vol. 5855, pp. 559–562.
[8] K. Y. Song, S. Chin, N. Primerov, and L. Thévenaz, "Time-domain distributed fiber sensor with 1 cm spatial resolution based on Brillouin dynamic grating," *J. Lightw. Technol.*, vol. 28, no. 14, pp. 2062–2067, Jul. 2010.
[9] W. Li, X. Bao, Y. Li, and L. Chen, "Differential pulse-width pair BOTDA for high spatial resolution sensing," *Opt. Exp.*, vol. 16, no. 26, pp. 21616–21625, 2008.
[10] Y. Dong, X. Bao, and W. Li, "Differential Brillouin gain for improving the temperature accuracy and spatial resolution in a long-distance distributed fiber sensor," *Appl. Opt.*, vol. 48, no. 22, pp. 1229–1235, 2009.
[11] Y. Dong, H. Zhang, L. Chen, and X. Bao, "2 cm spatial-resolution and 2 km range Brillouin optical fiber sensor using a transient differential pulse pair," *Appl. Opt.*, vol. 51, no. 9, pp. 1229–1235, 2012.

[12] M. A. Soto, M. Taki, G. Bolognini, and F. D. Pasquale, "Optimization of a DPP-BOTDA sensor with 25 cm spatial resolution over 60 km standard single-mode fiber using Simplex codes and optical pre-amplification," *Opt. Exp.*, vol. 20, no. 7, pp. 6860–6869, 2012.
[13] X. Angulo-Vinuesa, S. Martin-Lopez, P. Corredera, and M. Gonzalez-Herraez, "Raman-assisted Brillouin optical time-domain analysis with sub-meter resolution over 100 km," *Opt. Exp.*, vol. 20, no. 11, pp. 12147–14154, 2012.
[14] Y. Dong *et al.*, "High-spatial-resolution fast BOTDA for dynamic strain measurement based on differential double-pulse and second-order sideband of modulation," *IEEE Photon. J.*, vol. 5, no. 3, 2013, Art. no. 2600407.
[15] M. A. Soto, S. L. Floch, and L. Thévenaz, "Bipolar optical pulse coding for performance enhancement in BOTDA sensors," *Opt. Exp.*, vol. 21, no. 14, pp. 16390–16397, 2013.
[16] A. Minardo, A. Coscetta, L. Zeni, and R. Bernini, "High-spatial resolution DPP-BOTDA by real-time balanced detection," *IEEE Photon. Technol. Lett.*, vol. 26, no. 12, pp. 1251–1254, Jun. 2014.
[17] S. Diakaridia *et al.*, "Detecting cm-scale hot spot over 24-km-long single-mode fiber by using differential pulse pair BOTDA based on double-peak spectrum," *Opt. Exp.*, vol. 25, no. 15, pp. 17727–17736, 2017.
[18] H. Liang, W. Li, N. Linze, L. Chen, and X. Bao, "High-resolution DPP-BOTDA over 50 km LEAF using return-to-zero coded pulses," *Opt. Lett.*, vol. 35, no. 10, pp. 1503–1505, 2015.
[19] M. A. Farahani, E. Castillo-Guerra, and B. G. Colpitts, "A detailed evaluation of the correlation-based method used for estimation of the brillouin frequency shift in BOTDA sensors," *IEEE Sens. J.*, vol. 13, no. 12, pp. 4589–4598, Dec. 2013.
[20] A. K. Azad, L. Wang, N. Guo, C. Lu, and H. Y. Tam, "Temperature sensing in BOTDA system by using artificial neural network," *Electron. Lett.*, vol. 20, no. 51, pp. 1578–1580, 2015.
[21] A. K. Azad, L. Wang, N. Guo, H. Y. Tam, and C. Lu, "Signal processing using artificial neural network for BOTDA sensor system," *Opt. Exp.*, vol. 24, no. 6, pp. 6769–6782, 2016.
[22] H. Wu, L. Wang, N. Guo, C. Shu, and C. Lu, "Brillouin optical time domain analyzer assisted by support vector machine for ultrafast temperature extraction," *J. Lightw. Technol.*, vol. 35, no. 19, pp. 4159–4167, Oct. 2017.
[23] H. Wu, L. Wang, N. Guo, C. Shu, and C. Lu, "Support vector machine assisted BOTDA utilizing combined Brillouin gain and phase information for enhanced sensing accuracy," *Opt. Exp.*, vol. 25, no. 25, pp. 31210–31220, 2017.
[24] V. Vapnik, *The Nature of Statistical Learning Theory*. New York, NY, USA: Springer, 2013.
[25] C. Hsu and C. Lin, "A comparison of methods for multiclass support vector machines," *IEEE Trans. Neural Netw.*, vol. 13, no. 2, pp. 415–425, Mar. 2002.
[26] I. T. Jolliffe, *Principal Component Analysis*. New York, NY, USA: Springer, 2002.
[27] A. K. Azad, F. N. Khan, W. H. Alarashi, N. Guo, A. P. Lau, and C. Lu, "Temperature extraction in Brillouin optical time-domain analysis sensors using principal component analysis based pattern recognition," *Opt. Exp.*, vol. 25, no. 14, pp. 16534–16549, 2017.
[28] R. Ruiz-Lombera, A. Fuentes, L. Rodriguez-Cobo, J. M. Lopez-Higuera, and J. Mirapeix, "Simultaneous temperature and strain discrimination in a conventional BOTDA via artificial neural networks," *J. Lightw. Technol.*, vol. 36, no. 11, pp. 2114–2121, Jun. 2018.
[29] D. Zhou *et al.*, "Single-shot BOTDA based on an optical chirp chain probe wave for distributed ultra-fast measurement," *Light: Sci. Appl.*, vol. 7, May 11, 2018, Art. no. 32, DOI: 10.1038/s41377-018-0030-0.